

Locations of Roberge-Weiss transition endpoints in lattice QCD with $N_f = 2$ improved KS quarks

Liang-Kai Wu*

Faculty of Science, Jiangsu University, Zhenjiang 212013, Peoples Republic of China

Xiang-Fei Meng

National Supercomputer Center in Tianjin, Tianjin, 300457, Peoples Republic of China

(Dated: October 12, 2018)

Result on the locations of the tricritical points of $N_f = 2$ lattice QCD with imaginary chemical potential is presented. Simulations are carried out with Symanzik improved gauge action and Asqtad fermion action. With imaginary chemical potential $i\mu_I = i\pi T$, previous studies show that the Roberge-Weiss (RW) transition endpoints are triple points at both large and small quark masses, and second order transition points at intermediate quark masses. The triple and second order endpoints are separated by two tricritical ones. Our simulations are carried out at 7 values of quark mass am ranging from 0.024 to 0.070 on lattice volume $12^3 \times 4, 16^3 \times 4, 20^3 \times 4$. The susceptibility and Binder cumulant of the imaginary part of Polyakov loop are employed to determine the nature of RW transition endpoints. The simulations suggest that the two tricritical points are within the range 0.024 – 0.026 and 0.040 – 0.050, respectively.

PACS numbers: 12.38.Gc, 11.10.Wx, 11.15.Ha, 12.38.Mh

I. INTRODUCTION

The phase diagram of QCD has significantly phenomenological implications. It is relevant to the early Universe, compact stars and heavy ion collision experiments. Reviews on the study of phase diagram can be found in Refs. [1, 2] and references therein. While substantial lattice simulation has focused on the phase of QCD at finite density, a great amount of study centres around QCD with imaginary chemical potential. QCD with imaginary chemical potential has a rich phase structure, and it not only deserves detailed investigations in its own right theoretically, but also has significant relevance to physics at zero or small real chemical potential [3–11].

The $Z(3)$ symmetry which is present in the pure gauge theory is explicitly broken at the presence of dynamical quarks. However, Ref. [12] shows that the $Z(3)$ symmetry is restored when imaginary chemical potential is turned on and $Z(3)$ transformation can be compensated by a shift in μ_I/T by $2\pi/3$, so the partition function of QCD with imaginary chemical potential has periodicity in μ_I/T with period $2\pi/N_c$ as well as reflection symmetry in $\mu = i\mu_I$.

Different $Z(3)$ sectors are distinguished by the phase of Polyakov loop. At high temperature, the spontaneous breaking of $Z(3)$ symmetry implies transition between adjacent $Z(3)$ sectors in μ_I and this transition is of first order, while at low temperature, unbroken $Z(3)$ symmetry guarantees the transition is analytic. The first order transition takes place at those critical values of imaginary chemical potential $\mu_I/T = (2n + 1)\pi/3$ [12–14]. At high temperature, those first order transition points form

a transition line which necessarily ends at an endpoint T_{RW} when the temperature is decreased sufficiently low.

Recent numerical studies [3–5, 15, 16] show that the RW transition endpoints are triple points for small and heavy quark masses, and second order points for intermediate quark masses. So there exist two tricritical points separating the first order transition points from the second ones. Moreover, it is pointed out [3, 10, 11] that the scaling behaviour at the tricritical points may shape the critical line which separate different transition region for real chemical potential, and thus, the critical line for real chemical potential is expected to be qualitatively consistent with the scenario suggested in Refs. [17, 18] which shows that the first order transition region shrinks with increasing real chemical potential. In addition, Ref. [19] employs the scaling behaviour at the tricritical point to determine the nature of 2 flavour QCD transition in the chiral limit.

So far, the investigation for the Roberge-Weiss transition endpoints are implemented through standard gauge and fermion actions. In this paper, we aim to investigate the endpoints of $N_f = 2$ QCD with one-loop Symanzik-improved gauge action [20–23] and Asqtad KS action [24, 25]. These actions have discretization error of $O(\alpha_s^2 a^2, a^4)$ and $O(\alpha_s a^2, a^4)$, respectively. These improvements are significant on $N_t = 4$ lattice where the lattice spacing is quite large. Standard KS fermions suffer from taste symmetry breaking at nonzero lattice spacing a [26]. This taste symmetry breaking can be illustrated by the smallest pion mass taste splitting which is comparable to the pion mass even at lattice spacing $a \sim 0.1 fm$ [27]. Asqtad KS action has good taste symmetry and free dispersion relation by introducing fattened links and the so-called "Naik terms" [28, 29].

The paper is organized as follows. In Sec. II, we define the lattice action with imaginary chemical potential and

*Corresponding author. Email address: wuliangkai@163.com

the physical observables we calculate. Our simulation results are presented in Sec. III followed by discussions in Sec. IV.

II. LATTICE FORMULATION WITH IMAGINARY CHEMICAL POTENTIAL

After introducing pseudofermion field Φ , the partition function of the system can be represented as:

$$Z = \int [dU][d\Phi^*][d\Phi] e^{-S_g - S_f},$$

where S_g is the Symanzik-improved gauge action, and S_f is the Asqtad quark action with the quark chemical potential μ . Here $\mu = i\mu_I$. For S_g , we use

$$S_G = \beta \left(C_P \sum_{x;\mu<\nu} (1 - P_{\mu\nu}) + C_R \sum_{x;\mu\neq\nu} (1 - R_{\mu\nu}) + C_T \sum_{x;\mu<\nu<\sigma} (1 - T_{\mu\nu\sigma}) \right),$$

with $P_{\mu\nu}$, $R_{\mu\nu}$ and $T_{\mu\nu\sigma}$ standing for 1/3 of the imaginary part of the trace of 1×1 , 1×2 planar Wilson loops and $1 \times 1 \times 1$ "parallelogram" loops, respectively.

$$P_{\mu\nu} = \frac{1}{3} \text{ReTr} \left[\begin{array}{c} \text{---} \leftarrow \\ \leftarrow \text{---} \\ \leftarrow \text{---} \\ \text{---} \rightarrow \end{array} \right],$$

$$R_{\mu\nu} = \frac{1}{3} \text{ReTr} \left[\begin{array}{c} \text{---} \leftarrow \text{---} \\ \leftarrow \text{---} \text{---} \\ \leftarrow \text{---} \text{---} \\ \text{---} \rightarrow \text{---} \end{array} \right],$$

$$T_{\mu\nu\sigma} = \frac{1}{3} \text{ReTr} \left[\begin{array}{c} \text{---} \leftarrow \text{---} \\ \leftarrow \text{---} \text{---} \\ \leftarrow \text{---} \text{---} \\ \text{---} \rightarrow \text{---} \end{array} \right].$$

The coefficients C_P, C_R, C_T are tadpole improved [27],

$$\begin{aligned} C_P &= 1.0, \\ C_R &= \frac{-1}{20u_0^2} (1 - (0.6264 - 1.1746n_f) \ln(u_0)), \\ C_T &= \frac{1}{u_0^2} (0.0433 - 0.0156n_f) \ln(u_0). \end{aligned}$$

The Asqtad action with pseudofermion field Φ is

$$S_f = \left\langle \Phi \left| [M^\dagger[U]M[U]]^{-n_f/4} \right| \Phi \right\rangle,$$

where the form of $M_{x,y}[U] = 2m_{x,y} + D_{x,y}(U)$ reading

$$\begin{aligned} &2m\delta_{x,y} + \sum_{\rho=1}^3 \eta_{x,\rho} \left(U_{x,\rho}^F \delta_{x,y-\hat{\rho}} - U_{x-\hat{\rho},\rho}^{F\dagger} \delta_{x,y+\hat{\rho}} \right) \\ &+ \eta_{x,4} \left(e^{ia\mu_I} U_{x,4}^F \delta_{x,y-\hat{4}} - e^{-ia\mu_I} U_{x-\hat{4},\mu}^{F\dagger} \delta_{x,y+\hat{4}} \right) \\ &+ \sum_{\rho=1}^3 \eta_{x,\rho} \left(U_{x,\rho}^L \delta_{x,y-3\hat{\rho}} - U_{x-\rho,\rho}^{L\dagger} \delta_{x,y+3\hat{\rho}} \right) \\ &+ \eta_{x,4} \left(e^{i3a\mu_I} U_{x,4}^L \delta_{x,y-3\hat{4}} - e^{-i3a\mu_I} U_{x-\hat{4},\mu}^{L\dagger} \delta_{x,y+3\hat{4}} \right), \end{aligned}$$

where $U_{x,\rho}^F$ stands for the fattened link which is produced by Fat7 smearing and $U_{x,\rho}^L$ stands for the link term. $\hat{\rho}, \hat{4}$ are the unit vector along ρ -direction, 4-direction, respectively. $\eta_{x,\mu}$ is the staggered fermion phase.

We carry out simulations at $\theta = \mu_I/T = \pi$. As it is pointed out that the system is invariant under the charge conjugation at $\theta = 0, \pi$, when θ is fixed [9]. But the θ -odd quantity $O(\theta)$ is not invariant at $\theta = \pi$ under charge conjugation. When $T < T_{RW}$, $O(\theta)$ is a smooth function of θ , so it is zero at $\theta = \pi$. Whereas when $T > T_{RW}$, the two charge violating solutions cross each other at $\theta = \pi$. Thus the charge symmetry is spontaneously broken there and the θ -odd quantity $O(\theta)$ can be taken as order parameter. In this paper, we take the imaginary part of Polyakov loop as the order parameter.

The expression of Polyakov loop L is defined as the following:

$$\langle L \rangle = \left\langle \frac{1}{3L_s^3 L_t} \sum_{\mathbf{x}} \text{Tr} \left[\prod_{t=1}^{L_t} U_4(\mathbf{x}, t) \right] \right\rangle,$$

L_s, L_t are the spatial, time extent of lattice, respectively. To simplify notation, we use X to represent the imaginary part of Polyakov loop $\text{Im}(L)$. The susceptibility of imaginary part of Polyakov loop $\text{Im}(L)$ is defined as

$$\chi = L_s^3 \langle (X - \langle X \rangle)^2 \rangle,$$

which is expected to scale as: [4, 5]

$$\chi = L_s^{\gamma/\nu} \phi(\tau L_s^{1/\nu}), \quad (1)$$

where τ is the reduced temperature $\tau = (T - T_{RW})/T_{RW}$. This means that the curves $\chi/L_s^{\gamma/\nu}$ at different lattice volume should collapse with the same curve when plotted against $\tau L_s^{1/\nu}$. In the following, we employ $\beta - \beta_{RW}$ in place of $\tau = (T - T_{RW})/T_{RW}$. The critical exponents relevant to our study are collected in Table. I [5, 30].

We also consider the Binder cumulant of imaginary part of Polyakov loop which is defined as the following:

$$B_4 = \langle (X - \langle X \rangle)^4 \rangle / \langle (X - \langle X \rangle)^2 \rangle^2 \quad (2)$$

with $\langle X \rangle = 0$. In the vicinity of the RW transition line endpoints, B_4 with the finite size correction is a function of $x = (\beta - \beta_{RW})L_s^{1/\nu}$ and can be expanded as a series [3, 10, 11],

$$B_4 = B_4(\beta_c, \infty) + a_1 x + a_2 x^2 + \dots \quad (3)$$

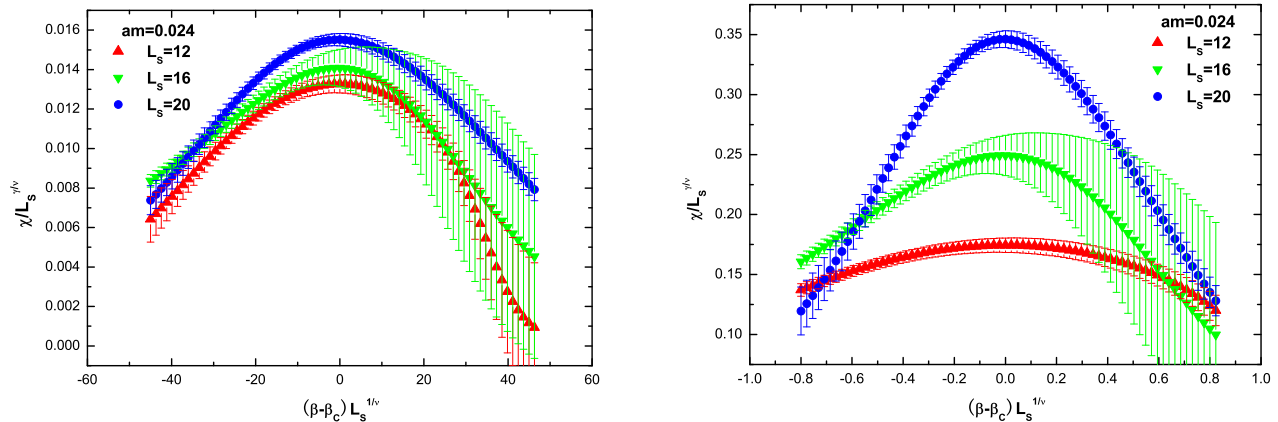


FIG. 1: Scaling behavior of the susceptibility of imaginary part of Polyakov loop according to first order critical index (left panel), and to 3D Ising critical index (right panel) at $am = 0.024$.

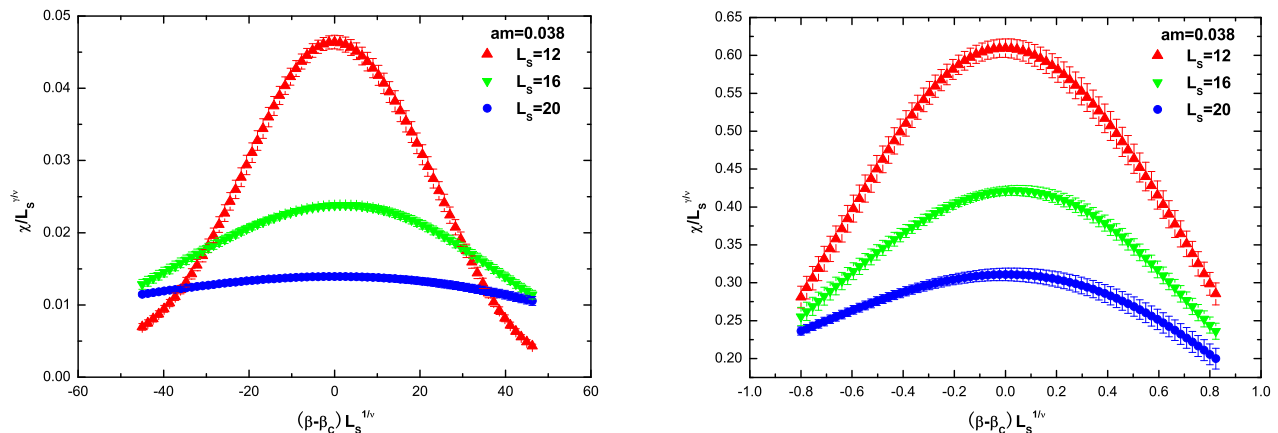


FIG. 2: Scaling behavior of the susceptibility of imaginary part of Polyakov loop according to first order critical index (left panel), and to 3D Ising critical index (right panel) at $am = 0.038$.

	$B_4(\beta_c, \infty)$	ν	γ	γ/ν
3D ising	1.604	0.6301(4)	1.2372(5)	1.963
tricritical	2	1/2	1	2
first order	1.5	1/3	1	3
crossover	3	-	-	-

TABLE I: Critical exponents relevant to our study.

In the thermodynamic limit, the critical index ν and $B_4(\beta_c, \infty)$ takes on the corresponding value summarized in Table. I. However, on finite spatial volumes, the steps of $B_4(\beta_c, \infty)$ are smeared out to continuous functions.

III. MC SIMULATION RESULTS

Before presenting the simulation results, we describe the simulation details. Simulations are carried out at quark mass $am = 0.024, 0.026, 0.038, 0.040, 0.050, 0.060, 0.070$. Rational Monte Carlo algorithm [31–33] is used to generate configurations. The Omelyan integration algorithm [34, 35] is employed for the gauge and fermion action. For the molecular dynamics evolution we use a 9'th rational function to approximate $[M^+(U)M(U)]^{-n_f/4}$ for the pseudofermion field. For the heat bath updating and for computing the action at the beginning and end of the molecular dynamics trajectory 10'th rational function is used to approximate $[M^+(U)M(U)]^{n_f/8}$ and $[M^+(U)M(U)]^{-n_f/8}$, respectively. The step is chosen to ensure the acceptance rate is around 80% – 90%. 5,000 trajectories of configu-

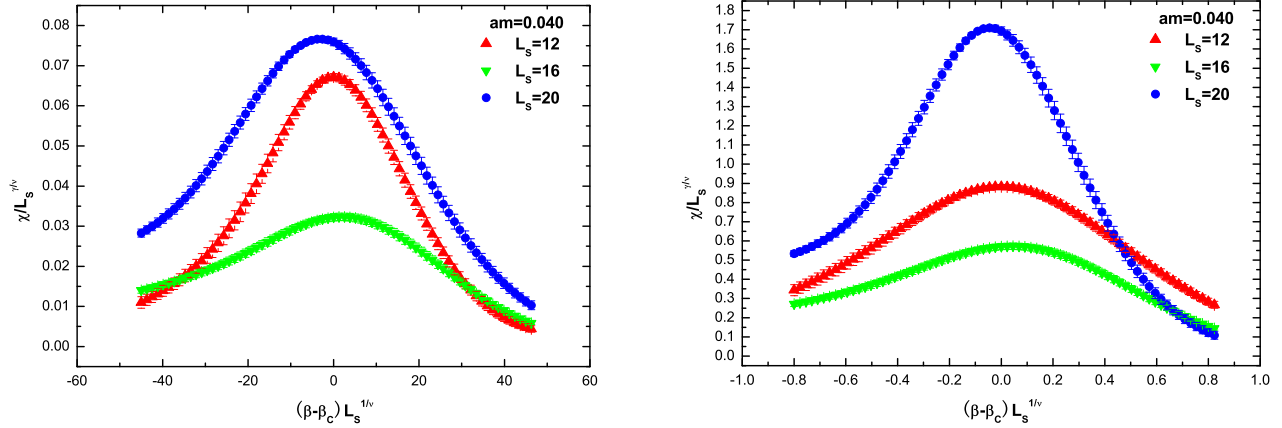


FIG. 3: Scaling behavior of the susceptibility of imaginary part of Polyakov loop according to first order critical index (left panel), and to 3D Ising critical index (right panel) at $am = 0.040$.

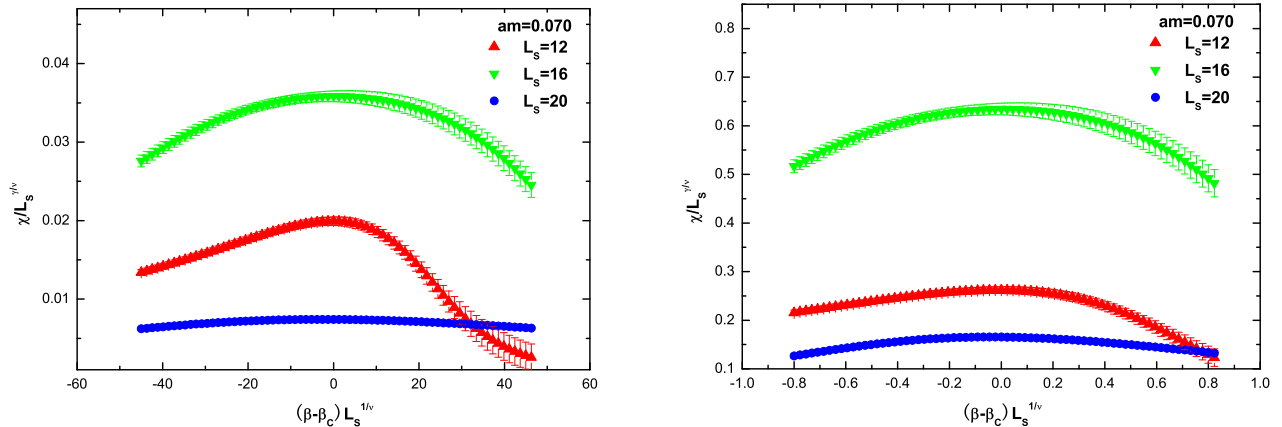


FIG. 4: Scaling behavior of the susceptibility of imaginary part of Polyakov loop according to first order critical index (left panel), and to 3D Ising critical index (right panel) at $\kappa = 0.070$.

ration are taken as warmup form a cold start. In order to fill in observables at additional β values, we employ the Ferrenberg-Swendsen reweighting method [36].

The critical coupling β_{RW} 's on various spatial volume at different quark mass am are summarized in Table. II. These β_{RW} 's are determined from the locations of peak susceptibility of imaginary part of Polyakov loop.

We present the rescaling susceptibility of imaginary part of Polyakov loop $\chi/L_s^{\gamma/\nu}$ as a function of $(\beta - \beta_{RW})L_s^{1/\nu}$ at $am = 0.024$ in Fig. 1. From Fig. 1, we can find that $\chi/L_s^{\gamma/\nu}$ according to the first order transition index collapses with the same curve, while $\chi/L_s^{\gamma/\nu}$ according to 3D index does not.

The rescaling susceptibility of imaginary part of Polyakov loop $\chi/L_s^{\gamma/\nu}$ as a function of $(\beta - \beta_{RW})L_s^{1/\nu}$ at $am = 0.038$ is depicted in Fig. 2. From Fig. 2, we

TABLE II: Results of critical couplings β_{RW} on different spatial volume at different κ .

am	12	16	20
0.024	6.492(9)	6.491(8)	6.4834(15)
0.038	6.838(4)	6.821(4)	6.824(3)
0.040	6.839(3)	6.839(3)	6.847(2)
0.050	6.845(10)	6.831(7)	6.857(4)
0.060	6.859(9)	6.865(14)	6.860(3)
0.070	6.875(7)	6.885(6)	6.857(4)

can find that $\chi/L_s^{\gamma/\nu}$ according to the first order transition index or 3D index does not collapse with the same

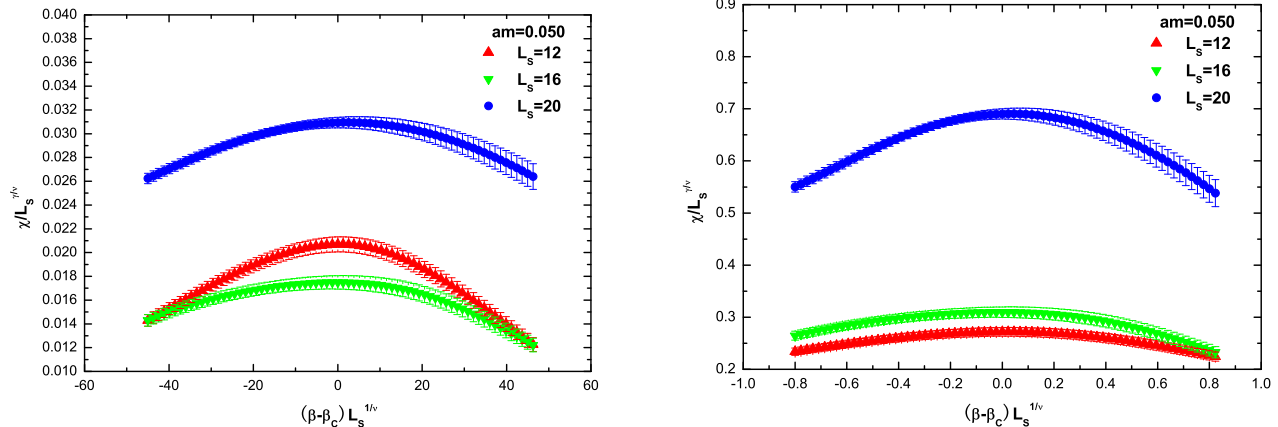


FIG. 5: Scaling behavior of the susceptibility of imaginary part of Polyakov loop according to first order critical index (left panel), and to 3D Ising critical index (right panel) at $\kappa = 0.050$.

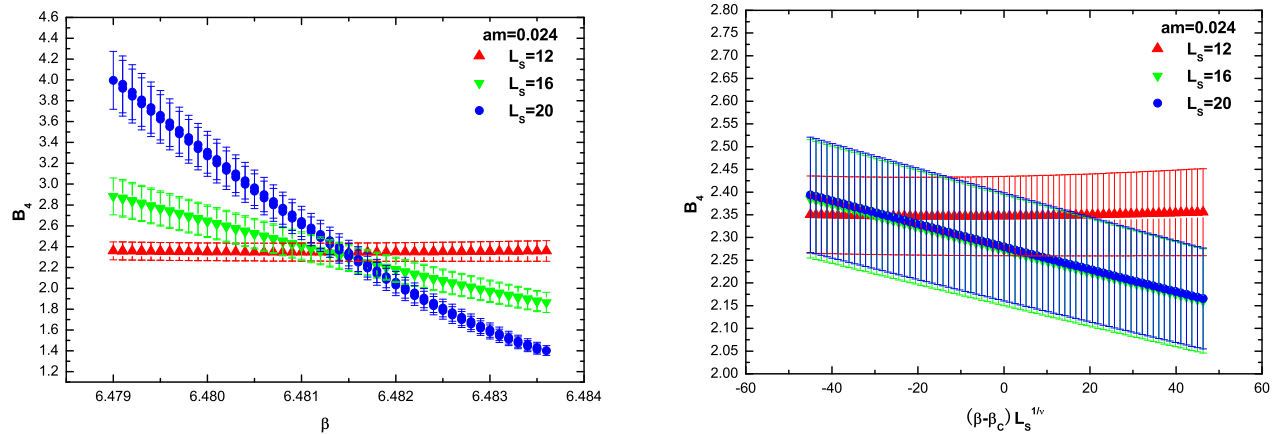


FIG. 6: Binder cumulants as a function of β on various spatial volume intersect at one point (left panel), and as a function of $(\beta - \beta_c)L_s^{1/\nu}$ with values of β_c, ν from Table. III collapse (right panel) at $am = 0.024$.

curve. We cannot determine the nature of Roberge-Weiss transition endpoint at $am = 0.038$ from $\chi/L_s^{\gamma/\nu}$.

The behaviour of rescaling susceptibility of imaginary part of Polyakov loop $\chi/L_s^{\gamma/\nu}$ at $am = 0.040$ and $am = 0.070$ are presented in Fig. 3, and Fig. 4 respectively. From Fig. 3 and Fig. 4, we can find that The rescaling susceptibility of imaginary part of Polyakov loop $\chi/L_s^{\gamma/\nu}$ at $am = 0.040$ and $am = 0.070$ have similar behaviour to the that at $am = 0.038$.

The rescaling susceptibility of imaginary part of Polyakov loop $\chi/L_s^{\gamma/\nu}$ as a function of $(\beta - \beta_{RW})L_s^{1/\nu}$ at $am = 0.050$ is depicted in Fig. 5. From Fig. 5, we can find that $\chi/L_s^{\gamma/\nu}$ as a function of $(\beta - \beta_{RW})L_s^{1/\nu}$ at lattice $12^3 \times 4$ and $16^3 \times 4$ are in favour of both first order transition index and 3D index. However, considering

the the scale of $\chi/L_s^{\gamma/\nu}$ and $(\beta - \beta_{RW})L_s^{1/\nu}$ in Fig. 5, the first order transition index may be the better choice. $\chi/L_s^{\gamma/\nu}$ as a function of $(\beta - \beta_{RW})L_s^{1/\nu}$ at $am = 0.060$ has similar behaviour to that at $am = 0.050$ which tends to be in favour of first order transition index.

In order to discern the scaling behaviour, we turn to investigate Binder cumulant B_4 as defined in Eq. (2) whose scaling behaviour is described in Eq. (3). B_4 decreases with the increase of β , and at one fixed quark mass am , B_4 as a function of β on various spatial volume is expected to intersect at one point. The intersection gives an estimate of accurate location of β_{RW} . By fitting to Eq. (3), we can extract critical index ν , β_{RW} and $B_4(\beta_c, \infty)$. The results are collected in Table. III.

We present B_4 as a function of β at $am = 0.024$ in the left panel of Fig. 6, and B_4 as a function of $(\beta -$

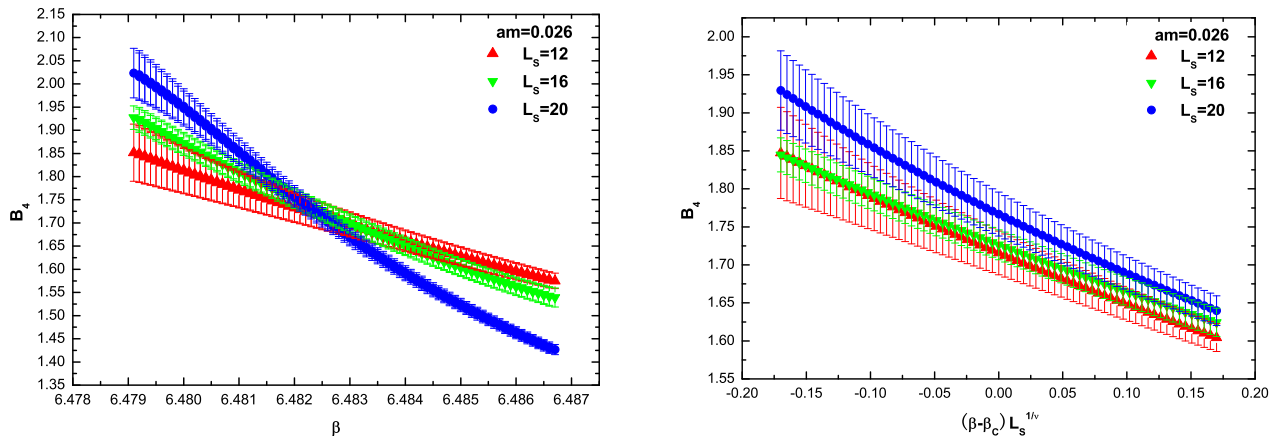


FIG. 7: Binder cumulants as a function of β on various spatial volume intersect at one point (left panel), and as a function of $(\beta - \beta_c)L_s^{1/\nu}$ with values of β_c, ν from Table. III collapse (right panel) at $am = 0.026$.

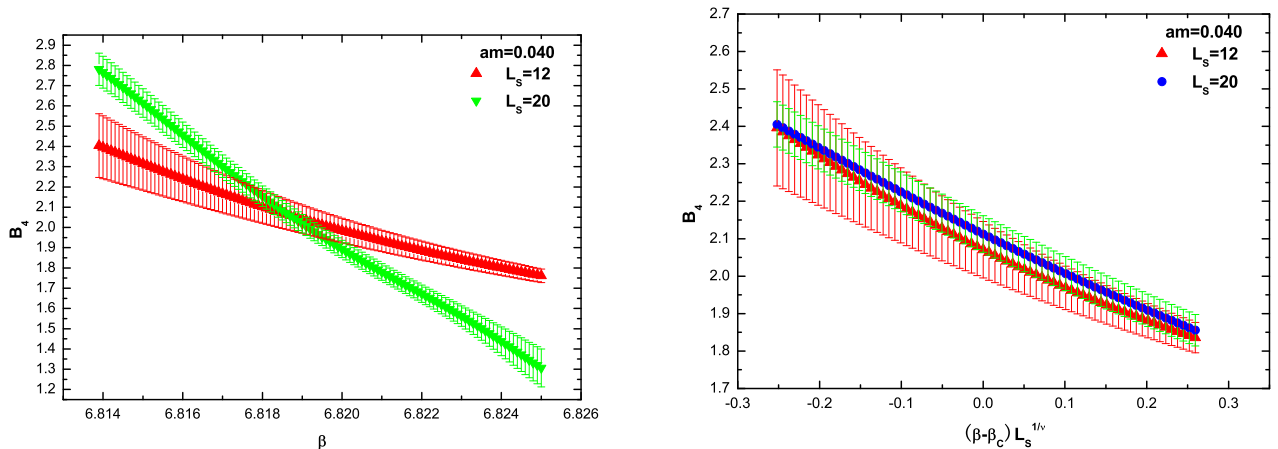


FIG. 8: Binder cumulants as a function of β on various spatial volume intersect at one point (left panel), and as a function of $(\beta - \beta_c)L_s^{1/\nu}$ with values of β_c, ν from Table. III collapse (right panel) at $am = 0.040$.

$\beta_{RW})L_s^{1/\nu}$ in the right panel of Fig. 6 with ν taken to be the extracted value through fitting procedure. From Table. III, we find that the critical index $\nu = 0.2410$ at $am = 0.024$ can explain the behaviour of B_4 as a function of $(\beta - \beta_{RW})L_s^{1/\nu}$, especially, on lattice $L_s = 16, 20$. This behaviour implies that the transition endpoint at $am = 0.024$ belongs to first order transition.

We also present B_4 as a function of β at $am = 0.026$ in the left panel of Fig. 7, and B_4 as a function of $(\beta - \beta_{RW})L_s^{1/\nu}$ in the right panel of Fig. 7 with ν taken to be the extracted value through fitting procedure. We find that the critical index $\nu = 0.6282$ at $am = 0.026$ can explain the behaviour of B_4 as a function of $(\beta - \beta_{RW})L_s^{1/\nu}$. $\nu = 0.6282$ suggests that the endpoint at $am = 0.026$ is of 3D transition nature.

At $am = 0.040$, we only find that B_4 as a function of β on lattice $L_s = 12, 20$ intersects at one point. B_4 as a function of β and as a function of $(\beta - \beta_{RW})L_s^{1/\nu}$ at $am = 0.040$ are depicted in the left, right panel of Fig. 7, respectively. The extracted value $\nu = 0.6173$ through fitting procedure also shows that the endpoint at $am = 0.040$ is of 3D transition nature. At other values of am , B_4 as a function of β and as a function of $(\beta - \beta_{RW})L_s^{1/\nu}$ have similar behaviour. For clarity, they are not presented.

From the behaviour of $\chi/L_s^{\gamma/\nu}$ and B_4 , we conclude that the nature of endpoint transition at $am = 0.024, 0.050, 0.060, 0.070$ is of first order, while at $am = 0.026, 0.038, 0.040$, the endpoint transition nature is of 3D Ising class. This conclusion suggests that the two tricritical

TABLE III: Results of critical couplings β_{RW} and the critical index ν by fitting Eq. (3) to data on different spatial volume. If errors are very small, we take them to be zero.

am	L_s	β_{RW}	ν	$B_4(\beta_c, \infty)$	a_1	a_2	r-square
0.024	12, 16, 20	6.4816(0)	0.2410(8)	2.2661(11)	-0.0022(0)	0.000(0)	0.991
0.026	12, 16, 20	6.4825(0)	0.6282(3)	1.71958(6)	-0.7061(14)	0.2033(9)	0.996
0.038	16, 20	6.8503(0)	0.6473(17)	1.0300(0)	-0.0363(4)	0.01145(2)	0.996
0.040	12, 20	6.8185(0)	0.6173(4)	2.1039(3)	-1.053(3)	0.136(8)	0.998
0.050	12, 16, 20	6.831(0)	0.3691(6)	1.8924(2)	-0.0295(4)	0.0008(0)	0.992
0.060	12, 20	6.8416(0)	0.3458(19)	1.6937(10)	-0.0125(6)	-	0.958
0.070	12, 20	6.8416(0)	0.3152(6)	2.1821(2)	-0.005(0)	-	0.936

points are between $0.024 < am_{tricl} < 0.026$ and $0.040 < am_{tricl} < 0.050$.

IV. DISCUSSIONS

We have studied the nature of critical endpoints of Roberge-Weiss transition of two flavor lattice QCD with improved KS fermions. When $i\mu_I = i\pi T$, the imaginary part of Polayakov loop is the order parameter for studying the transition from low temperature phase to high temperature one.

Our simulations are carried out at 7 values of quark mass am on $L_t = 4$ lattice on different 3 spatial volumes. Our central result is that the two tricritical points are between $0.024 < am_{tricl} < 0.026$ and $0.040 < am_{tricl} < 0.050$. The interval of quark mass from 0.024 to 0.026 is narrow. On finite spatial volume, the index ν is expected to change smoothly, while our simulation shows that index ν changes rapidly within a narrow quark mass interval.

In Ref. [5], the two locations of tricritical point for $N_f = 2$ QCD are $am = 0.043(5), 0.72(8)$, respectively. For $N_f = 3$ QCD, Ref. [3] concludes that the two tricritical points are between $0.07 < am_{tricl} < 0.3$ and $0.5 < am_{tricl} < 1.5$. Comparing with those results, the second transition region from our simulation is narrow.

Apart from monitoring the behaviour of susceptibility of imaginary part of Polayakov loop $\text{Im}(L)$, we also look into the change of Binder cumulant of $\text{Im}(L)$. In order to fill in observables at additional β values, the Ferrenberg-Swendsen reweighting method [36] is employed. It is noted that when applying Ferrenberg-Swendsen reweighting method, the number of β points taken to calculate susceptibility is not completely the same as the number taken to calculate Binder cumulant.

In our simulations, the behaviour of susceptibility of imaginary part of Polayakov loop $\text{Im}(L)$ at $am = 0.024$

can give us clear signal to determine the nature of transition, while at other quark mass, it is difficult to determine the nature of transition.

The values of $B_4(\beta_c, \infty)$ extracted through fitting procedure are not in consistent with what are expected. This is because logarithmic scaling corrections will be present near the tricritical point [3, 37], and our simulations are carried out on finite size volume on which large finite size corrections are observed in simpler spin model [38]. However, the critical exponent ν is not sensitive to finite size corrections [3]. So index ν extracted through fitting procedure can provide us information to determine the transition nature.

In our simulation, we can find that the values of B_4 on lattice with spatial volumes $12^3, 16^3, 20^3$ intersect approximately at one point at quark masses $am = 0.024, 0.026, 0.050$, while at other quark mass, it is difficult to find intersection point for B_4 's from three spatial volumes. It is expedient to determine the intersection point from two spatial volumes as indicated in Table. III.

Taking what mentioned above into account, further work along this direction which can provide crosscheck is expected, especially simulations with larger time extent which is being under our consideration.

Acknowledgments

We thank Philippe de Forcrand for valuable helps. We modify the MILC collaboration's public code [39] to simulate the theory at imaginary chemical potential. We use the fortran-90 based multi-precision software [40]. This work is supported by the National Science Foundation of China (NSFC) under Grant Nos. (11347029). The work was carried out at National Supercomputer Center in Wuxi, We appreciate the help of Qiong Wang and Zhao liu when carrying out the computation.

[1] K. Fukushima and T. Hatsuda, Rept. Prog. Phys. **74** 014001 (2011).

[2] K. Fukushima, J. Phys. G **39** 013101 (2012).

- [3] P. de Forcrand and O. Philipsen, Phys. Rev. Lett. **105**, 152001 (2010) [arXiv:1004.3144 [hep-lat]].
- [4] M. D'Elia and F. Sanfilippo, Phys. Rev. D **80**, 111501 (2009) [arXiv:0909.0254 [hep-lat]].
- [5] C. Bonati, G. Cossu, M. D'Elia and F. Sanfilippo, Phys. Rev. D **83**, 054505 (2011) [arXiv:1011.4515 [hep-lat]].
- [6] M. D'Elia, F. Di Renzo and M. P. Lombardo, Phys. Rev. D **76**, 114509 (2007) [arXiv:0705.3814 [hep-lat]].
- [7] Y. Sakai, H. Kouno and M. Yahiro, J. Phys. G **37**, 105007 (2010) [arXiv:0908.3088 [hep-ph]].
- [8] G. Aarts, S. P. Kumar and J. Rafferty, JHEP **1007**, 056 (2010) [arXiv:1005.2947 [hep-th]].
- [9] H. Kouno, Y. Sakai, K. Kashiwa and M. Yahiro, J. Phys. G **36**, 115010 (2009) [arXiv:0904.0925 [hep-ph]].
- [10] O. Philipsen and P. de Forcrand, PoS LATTICE **2010**, 211 (2010) [arXiv:1011.0291 [hep-lat]].
- [11] C. Bonati, P. de Forcrand, M. D'Elia, O. Philipsen and F. Sanfilippo, PoS LATTICE **2011**, 189 (2011) [arXiv:1201.2769 [hep-lat]].
- [12] A. Roberge and N. Weiss, Nucl. Phys. B **275**, 734 (1986).
- [13] P. de Forcrand and O. Philipsen, Nucl. Phys. B **642**, 290 (2002).
- [14] M. D'Elia and M. -P. Lombardo, Phys. Rev. D **67**, 014505 (2003) [hep-lat/0209146].
- [15] O. Philipsen and C. Pinke, Phys. Rev. D **89**, no. 9, 094504 (2014) doi:10.1103/PhysRevD.89.094504 [arXiv:1402.0838 [hep-lat]].
- [16] L. K. Wu and X. F. Meng, Phys. Rev. D **90**, no. 9, 094506 (2014) doi:10.1103/PhysRevD.90.094506 [arXiv:1405.2425 [hep-lat]].
- [17] P. de Forcrand and O. Philipsen, JHEP **0701**, 077 (2007) [hep-lat/0607017].
- [18] P. de Forcrand and O. Philipsen, JHEP **0811**, 012 (2008) [arXiv:0808.1096 [hep-lat]].
- [19] C. Bonati, P. de Forcrand, M. D'Elia, O. Philipsen and F. Sanfilippo, Phys. Rev. D **90**, no. 7, 074030 (2014) doi:10.1103/PhysRevD.90.074030 [arXiv:1408.5086 [hep-lat]].
- [20] K. Symanzik, Nucl. Phys. B **226**, 187 (1983). doi:10.1016/0550-3213(83)90468-6
- [21] M. Luscher and P. Weisz, Phys. Lett. **158B**, 250 (1985). doi:10.1016/0370-2693(85)90966-9
- [22] G. P. Lepage and P. B. Mackenzie, Phys. Rev. D **48**, 2250 (1993) doi:10.1103/PhysRevD.48.2250 [hep-lat/9209022].
- [23] M. G. Alford, W. Dimm, G. P. Lepage, G. Hockney and P. B. Mackenzie, Phys. Lett. B **361**, 87 (1995) doi:10.1016/0370-2693(95)01131-9 [hep-lat/9507010].
- [24] T. Blum *et al.*, Phys. Rev. D **55**, 1133 (1997) doi:10.1103/PhysRevD.55.1133 [hep-lat/9609036].
- [25] K. Orginos *et al.* [MILC Collaboration], Phys. Rev. D **60**, 054503 (1999) doi:10.1103/PhysRevD.60.054503 [hep-lat/9903032].
- [26] A. Bazavov *et al.*, Phys. Rev. D **85**, 054503 (2012) doi:10.1103/PhysRevD.85.054503 [arXiv:1111.1710 [hep-lat]].
- [27] A. Bazavov *et al.* [MILC Collaboration], Rev. Mod. Phys. **82** 1349 (2010).
- [28] S. Naik, 1989 Nucl. Phys. B **316** 238 (1989).
- [29] C. W. Bernard *et al.* [MILC Collaboration], Phys. Rev. D **58** 014503 (1998).
- [30] A. Pelissetto and E. Vicari, Phys. Rept. **368**, 549 (2002) [cond-mat/0012164].
- [31] M. A. Clark and A. D. Kennedy, Nucl. Phys. Proc. Suppl. **129** 850 (2004).
- [32] M. A. Clark and A. D. Kennedy, Phys. Rev. D **75** 011502 (2007).
- [33] M. A. Clark and A. D. Kennedy, Phys. Rev. Lett. **98** 051601 (2007).
- [34] T. Takaishi and P. De Forcrand, Phys. Rev. E **73** 036706 (2006).
- [35] I. P. Omeylan, I. M. Mryglod and R. Folk, Comp. Phys. Comm. **151** 272 (2003).
- [36] A. M. Ferrenberg and R. H. Swendsen, Phys. Rev. Lett. **63**, 1195 (1989).
- [37] I.D. Lawrie and S. Sarbach, in *Phase transitions and critical phenomena*, eds. C. Domb and J.L. Lebowitz, vol.9, 1 (1984).
- [38] A. Billoire, T. Neuhaus and B. Berg, Nucl. Phys. B **396**, 779 (1993) [hep-lat/9211014].
- [39] <http://physics.utah.edu/~detar/milc/>
- [40] <http://crd-legacy.lbl.gov/~dhbailey/mpdist/>